Chapter 6

Effect of antisite disorder on the magnetic and transport properties of a quarternary Heusler alloy

6.1 Introduction

Researchers are actively studying Heusler alloys in the fields of spintronics and multifunctional quantum materials because of their favourable physical features and potential for creative applications. The Heusler family comprises a wide range of captivating magnetic materials, such as half-metallic ferromagnets (Bainsla et al. (2015b)), spin-gapless semiconductors (Bainsla et al. (2015a)), bipolar magnetic semiconductors (Nag et al. (2021)), and spin semimetals (Venkateswara et al. (2019)). These materials possess a stable structure, high spin polarization, and enhanced ordering temperatures, which sets them apart from other spintronic materials and makes them well-suited for many applications. According to their atomic arrangements, different types of systems are possible: Half Heusler (XYZ), full Heusler (X_2YZ), and quaternary Heusler alloys [QHAs] ($XX'YZ$). The X, X', and Y belong to the transition metal elements and Z belongs to the p-block element. Among all

the possible structures of Heusler alloys QHAs are composed of four different elements ($XX'YZ$) (Graf et al. (2011)), offering a rich playground for tailoring their physical and chemical characteristics. The presence of two distinct sublattices in quaternary Heusler alloys imparts numerous advantages, making these materials highly intriguing for scientific exploration and technological applications. One of the key advantages is that the electronic band structure, spin polarization, and magnetic moments can be selectively adjusted by manipulating the composition and arrangement of elements on the two sublattices. Among all the QHAs, the Co-based Heusler alloys have become a pivotal focus in research, driven by their notable attributes, including high Curie temperatures (T_C), remarkable spin polarization, and the ability to fine-tune electronic structures (Mouatassime et al. (2021); Nag et al. (2022)). Furthermore, these alloys typically exhibit a substantial anomalous Hall effect (AHE) (Xia et al. (2022)).

The definition of normal Hall effect is defined as when an external magnetic field is applied perpendicular to the current flow in a conductor, resulting in the formation of a transverse voltage (Šmejkal et al. (2022)). The anomalous Hall effect (AHE) is an observable phenomenon in materials that have broken time-reversal symmetry where an extra contribution to the transverse voltage is seen. The emergence of the anomalous Hall effect (AHE) may be attributed to the interaction between magnetization and spin-orbit coupling. The basic understanding of the observation of AHE suggests that it arises from the extrinsic and intrinsic mechanisms. The extrinsic mechanism includes the involvement of skew scattering and side jump mechanisms, which are related to the asymmetric scattering and transverse change of the propagation direction of spin-polarized charge carriers, respectively. On the other hand, the intrinsic mechanism is connected to the Berry curvature in momentum space that is related to the electronic band structure. Prompting both theoretical and experimental investigations to comprehend its fundamental origin, particularly concerning Berry curvature. Notably, certain Co-based

compounds within this category, such as $CrFeVGa$ (Nag et al. (2023)) and $CoFeVSb$ (Nag et al. (2022)), have been reported to display AHE associated with Berry curvature (Roy et al. (2020)). Interestingly, the skew scattering mechanism tends to be less prominent in these alloys, as it often makes a negligible contribution to the AHE. This emphasizes the need for a comprehensive understanding of the AHE in cobalt-based Heusler alloys, as it holds significant implications for their potential applications in spintronics and related technologies (Alijani et al. (2011)).

However, Heusler compounds, particularly QHAs, are susceptible to antisite disorder within the d-block elements, a characteristic accentuated by the presence of three different d-block elements in the formula. Antisite disorder, characterized by the substitution of atoms from one type for another within the crystal lattice, is a prevalent defect in Heusler alloys and can significantly influence their electronic, magnetic, and thermal properties. Notably, in QHAs, antisite disorder is strategically employed to tailor the electronic, magnetic, and transport properties of the system (Malik et al. (2022)). Previous studies on Co-based magnetic Heusler compounds initially suggested that antisite disorder might be unfavorable for increasing the Anomalous Hall Effect (AHE), with thin films like Co_2MnGa and Co_2MnAl exhibiting smaller σ_{xy}^{A} values compared to well-ordered single crystals (Markou et al. (2019); Sakuraba et al. (2020)). However, recent investigations have unveiled intriguing findings; an enhanced intrinsic AHC was observed in Fe2-based (Mende et al. (2021)) inverse Heusler compounds attributed to antisite disorder. Furthermore, in the Co_2FeAl Heusler compound, antisite disorder between Fe and Al atoms led to a Berry curvature-driven enhancement in intrinsic AHE. These findings underscore the nuanced role of antisite disorder in shaping the properties of Heusler alloys and offer avenues for tuning in advanced applications.

In the existing literature the CFMS system, with (Xia et al. (2023)) affirms its status as a half-metallic ferromagnet (HMF) through a combination of experimental and theoretical

data. Another independent investigation by (Gupta et al. (2023)) supports the spin-gapless semiconducting (SGS) nature of CFMS, both theoretically and through transport properties analysis. Notably, while the former study verifies the system's structural purity, the later reveals a slight deviation from stoichiometry. Additionally, the later study explores the impact of pressure on CFMS, observing a transformation from SGS to HMF under pressure. In this present study, we delve into the comprehensive characterization of the quaternary Heusler alloy system $CoFeMnSn$, employing structural, magnetic, and transport measurements. Our structural analysis confirms the presence of antisite disorder in the system. Further exploration focuses on understanding the influence of antisite disorder on the magnetic and transport properties of the system. Magnetization studies affirm the ferromagnetic nature of the CFMS system, while transport data reveals the presence of an anomalous Hall effect, attributed to an intrinsic mechanism associated with Berry curvature. This multifaceted investigation contributes valuable insights into the intricate interplay between structural disorder and the magnetic and transport behaviors of quaternary Heusler alloys.

6.2 Experimental Details

The Arc melting method is used to make the polycrystalline CFMS sample. The elements Co, Fe, Mn, and Sn with a purity of 99.95% were taken in a stoichiometric ratio i.e 1:1:1:1. The sample was melted several times to ensure homogeneity and then the melted ingot was sealed in a quartz tube under a base pressure of 10^{-6} mbar. The sealed quartz tube is further placed into the furnace at 1073 K for five days for the annealing process which is then followed by the quenching process in the ice water. The powder X-ray diffraction (XRD) of the system is performed after crushing the sample into the fine powder. The powder XRD was done using the Rigaku MiniFlex II DESKTOP powder diffractometer ($Cu\mathrm{K}_{\alpha}$ radiation, $\lambda = 1.54184$). The Rietveld refinement of the X-ray spectrum, is done

using the Fullprof software to determine the lattice parameter and atomic position of the system. For the transport study, a 1.28 mm $\times$ 0.62 mm $\times$ 0.23 mm rectangular piece is cut with a diamond cutter. The physical properties of the system are measured by the Physical Properties Measurement System (Quantum Design). For longitudinal resistivity (ρ_{xx}) four probe method is used for which the probe was made using the silver paste and gold wires. The current of magnitude 3 mA is applied in the X- direction and voltage is also measured in the X- direction. For magneto-transport the current is applied along X- direction and magnetic field (B) is applied perpendicular to the sample let say Z- direction and voltage is measured along the X- direction. The transverse resistivity (ρ_{xy}) is measured in which the voltage is measured along the Y-direction. The Magnetic measurements of the system were performed using a superconducting quantum interference device-based magnetometer (MPMS, Quantum Design).

6.3 Results and Discussions

6.3.1 XRD study

The crystal structure of bulk samples was determined through X-ray diffraction (XRD) measurements. Figure 6.1 displays the powder XRD of the CFMS system at room temperature (300 K). The quaternary Heusler alloy *CoFeMnSn* crystallizes in the *LiMgPdSn* prototype structure with space group F$\bar{4}$3m. The observed XRD, revealed clear characteristic peaks (220), (400), and (422) indicative of the cubic Heusler phase. Importantly, no diffraction peaks from impure phases were detected, ensuring the purity of the samples. Additionally, distinct superlattice diffraction peaks (111) and (200) are prominently featured in the XRD pattern, suggesting a notable degree of atomic ordering within these alloys. For refinement, three non-degenerate structures were considered in the case of quaternary ($XX'YZ$) Heusler alloys. In type I which was considered here in which the X, X', Y, and Z atom was placed

at 4c (0.25, 0.25, 0.25), 4d (0.75, 0.75, 0.75), 4b (0.5, 0.5, 0.5) and 4a (0,0,0) respectively. The structure factor formula for the quarternary Heusler alloy is formulated as:

$$F_{hkl} = 4 * \left(f_z + f_y e^{i\pi(h+k+l)} + f_x e^{\frac{i\pi}{2}(h+k+l)} + f_x e^{\frac{-i\pi}{2}(h+k+l)} \right) \tag{6.1}$$

Therefore,

$$F_{111} = 4[(f_z - f_y) - i(f_x - f_x)] \tag{6.2}$$

$$F_{200} = 4[(f_z + f_y) - (f_x + f_x)] \tag{6.3}$$

$$F_{220} = 4[(f_z + f_y) + (f_x + f_x)] \tag{6.4}$$

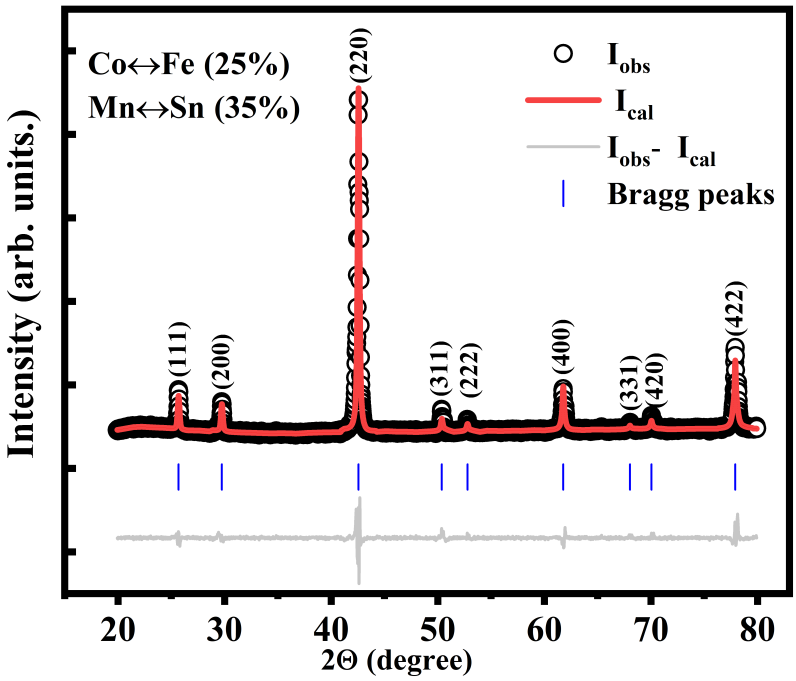

Fig. 6.1 Room temperature XRD pattern of *CoFeMnSn* along with the refinement for the Type I configuration with antisite disorder between *Co* and *Fe*, and *Mn* and *Sn*.

From the atomic structure formulae mentioned above in equations 6.2, 6.3 and 6.4 it was clear that the prominent presence of peaks (111) and (200) arose due to the antisite disorder between the $Co \leftrightarrow Fe$ and $Mn \leftrightarrow Sn$ respectively. The refinement of the system is

done after including the 25 % and 30 % antisite disorder between $Co \leftrightarrow Fe$ and $Mn \leftrightarrow Sn$ atoms respectively. The lattice constants for CFMS bulk were determined to be 6.0016 Å. Notably, the lattice parameter value is higher than the reported by Xia et al. because there is a disorder in the system caused by antisite defects.

6.3.2 SEM Analysis

The energy-dispersive spectra (EDS) for the CoFeMnSn sample are shown in the graphs in the figure 6.2, while the composition maps that were obtained from the EDS images are shown in the figure. The atomic percentages of the constituent elements are closely matched with the stoichiometric of the compound, viz., 1:1:1:1, within the experimental error of not more than 3 %. The occurrence of an antisite disorder between the two elements is implied by the fact that the atomic percentage of Sn is higher than that of Mn, which has a lower atomic value. Similar is the case with Co and Fe, the atomic percentage of Fe is higher than that of cobalt, which results in the possibility of an antisite disorder between the two elements.

6.3.3 X-ray absorption spectroscopy (XAS)

The electronic characteristics of the CFMS sample were investigated by conducting X-ray Absorption Spectroscopy (XAS) and X-ray Magnetic Circular Dichroism (XMCD) measurements on the Co, Fe, and Mn elements at 300 K. The XAS/XMCD spectra of Mn, Co and Fe-$L_{2,3}$ edge is shown in figure 6.3. The XAS spectrum of Mn shows the presence of two main peaks located at binding energies 638 eV and 651 eV. The absence of any multiplets in the L_3 and L_2 edge of the XAS spectra suggests the presence of the metallic nature of the elements in the system. In order to regain the information regarding magnetic ordering in the system the XMCD signal of the elements is also present lower pannel of figure 6.3. A negative dichroism signal was seen in the L_3 area, whereas a positive

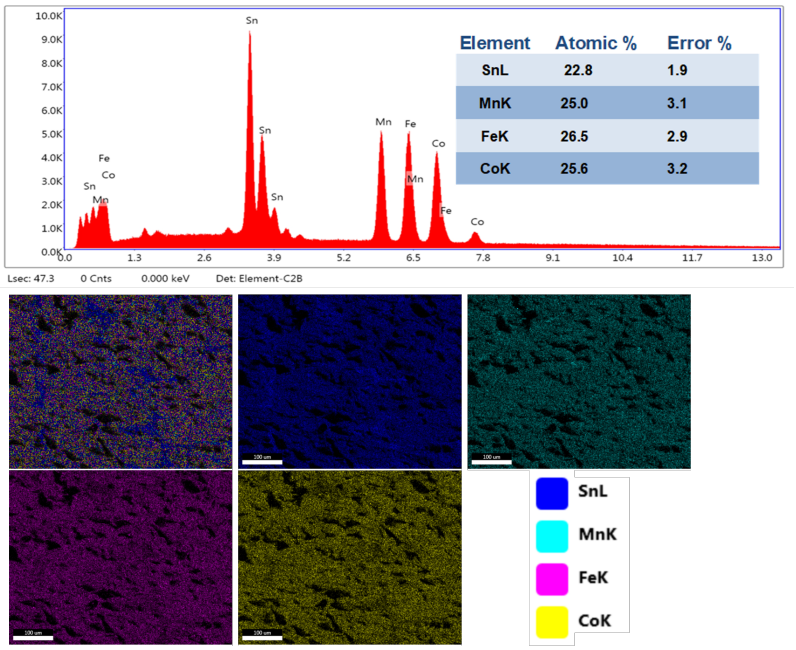

Fig. 6.2 Upper pannel shows the EDS spectrum of the constituent elements of CoFeMnSn (Inset shows the atomic percentage of respective elements) lower panel shows the composition mapping of constituent elements.

signal was observed in the L_2 region for Mn, Co, and Fe (see figure 6.3. The presence of a non-zero signal confirms the magnetic ordering of the elements. The observed disparity between the spectra suggests that the system did not undergo an oxidation state, indicating its pure nature. Additionally in the XAS/XMCD spectra of Co which is recorded at 300 K. The Co $L_{2,3}$ edge spectrum shows the presence of two main peaks at 777 eV and 793.5 eV. A shoulder peak is also observed at 3 eV higher binding energy. These structures correspond to the Heusler alloys due to the Co-Co bonding states within the molecular orbital calculations (Elmers et al. (2003); Telling et al. (2006)). The XAS/XMCD spectra have revealed that the magnetic moments of Mn, Co, and Fe are aligned in the same direction, hence confirming the ferromagnetic character of the system.

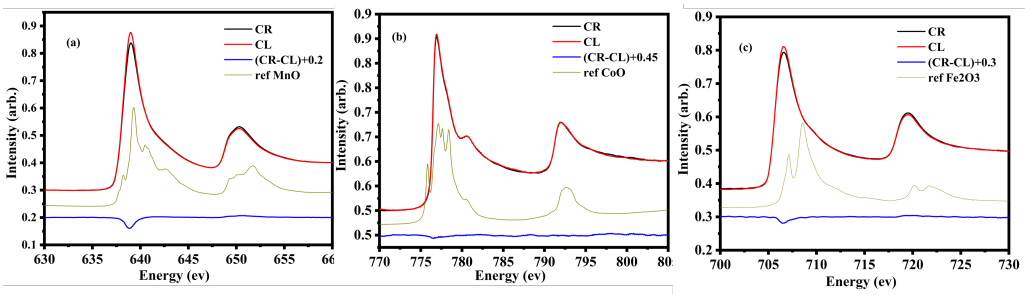

Fig. 6.3 The x-ray absorption spectra of Mn (a), Co (b), and Fe (c) along with the XMCD spectra of respective elements at 300 K

6.3.4 Isothermal Magnetization Study

To understand the effect of antisite disorder on the magnetic properties of the system the isothermal magnetization (M(H)) of the system is measured as shown in the figure 6.4. The M(H) increases at low field region and after it gets saturated, indicating that the system is ferromagnetic in nature. The magnitude of saturation magnetization for the CFMS system reported by Xia et. al. and gupta et al, was 4.16 $\mu_B/f.u.$ Which is within close agreement with the value obtained from slater pauling (S-P) rule. All known Heusler compounds adhere to a governing S-P rule. According to this rule, the total magnetic moment for a Heusler alloy can be calculated using the formula $m = (N_V - 24)\mu_B/f.u.$ In this equation, m represents the total magnetic moment, and N_V signifies the total valence electron count (VEC) of the compound (Graf et al. (2010)). Applying this rule to *CoFeMnSn*, with a total VEC of 28, the anticipated total magnetic moment, in accordance with the S-P rule, is expected to be 4 $\mu_B/f.u.$ But for the present system, the experimentally observed magnitude of Ms was 4.3$\mu_B/f.u.$ Which is much more than the calculated from S-P rule.

As observed here, the S-P rule is not being obeyed here, viz; for CFMS according to SP rule “Zt-24’. Here Zt= 24 for the present system and we observed non integer value instead of an integer value required for a Husler system to be half metallic or spin gapless in nature. Many studies have shown similar kind of discrepancies in the value of *Ms* (Nag et al. (2022); Venkateswara et al. (2023)). According to their investigation, the discrepancy

at the moment was due to the effect of antisite disorder between the magnetic entities. As Heusler alloys are formed with different combinations of d- d-block elements there was a huge possibility of the antisite disorder in the system. In the case of CFMS, all three elements are positioned next to each other in the periodic table so it may be concluded that the presence of antisite disorder in the system increases the saturation moment for the system. Hence, a non-integer value also indicates the fact that the present system does not show a halfmetallic or spin-gapless nature. In addition to this, the isothermal

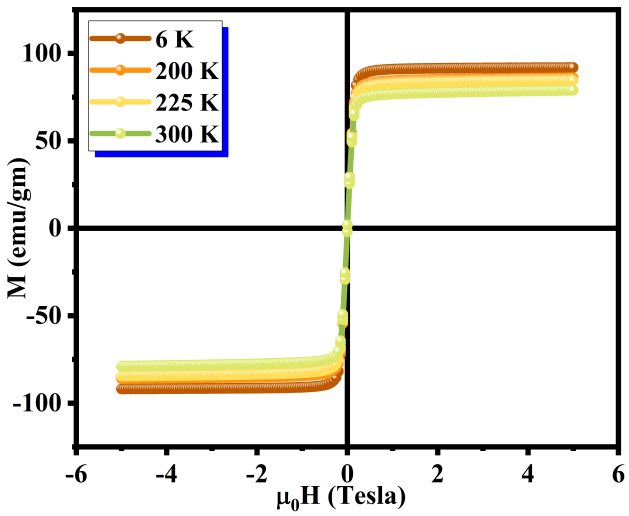

Fig. 6.4 Isothermal magnetization (M(H)) curve recorded at 6K and 300 K, dotted line shows the predicted value of ms from Slater Pauling rule.

magnetization (M(H)) measurements have been done at different temperatures up to an applied field of ± 50 kOe shown in figure 6.2. The M(H) indicated the ferromagnetic nature of the system. The magnetic moment decreased as the temperature increased from 2 K to 300 K. From M(H) data, it is clear that the system is ferromagnetic up to room temperature (RT) suggesting that the Curie temperature is well above the RT.

6.3.5 Transport properties

The figure 6.5 shows the temperature-dependent resistivity (ρ(T)) of the system. It shows that resistivity decreases as the temperature increases, suggesting semiconducting behavior. But it is also found that the value of resistivity does not change with temperature means weak temperature dependence. It shows a non-metallic behavior and the minor dependency on temperature eliminates its semiconducting behavior. A similar kind of behavior is observed for semimetallic compounds belonging to the Heusler family Mondal et al. (2018).

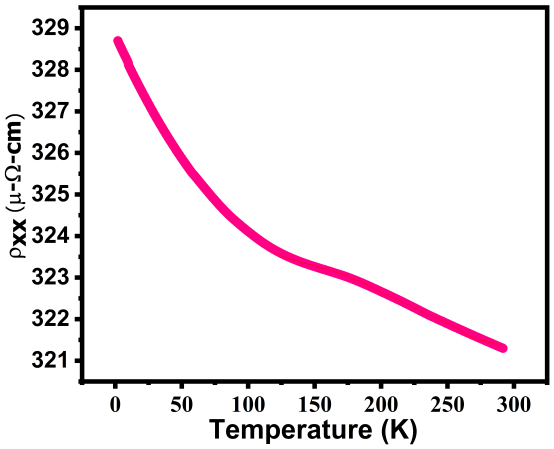

Fig. 6.5 Temperature dependent longitudinal electrical resistivity of the system

6.3.6 Hall Resistivity

To understand the effect of antisite disorder on the anomalous transport properties of the CFMS system, the Hall resistivity (ρ_{xy}) of the system was measured for different temperature ranges between 2 K to 300 K as shown in figure 6.6. The behavior of ρ_{xy} is analogous to the M (H) behavior, suggesting the presence of anomalous Hall effect (AHE)

in the system. Now, the total ρ_{xy} is explained by the following equation:

$$\rho_{xy} = R_o H + R_s M_s \tag{6.5}$$

Here, R_o, R_s is the ordinary, anomalous Hall coefficient respectively and M_s is the

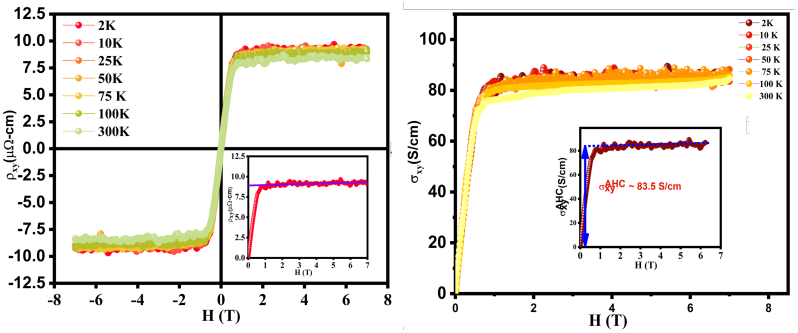

Fig. 6.6 (a) Field dependence of Hall resistivity at various temperatures (Inset showing the linear fit of Hall data at high field) (b) field dependent Hall resistivity at different temperatures (Inset showing the Anomalous Hall conductivity at 2K.)

magnetization of the system. The additional term $R_s M_s$ which is called AHE, is due to the magnetization of the system. In order to separate the contribution from the anomalous part, the contribution coming from the ordinary part is subtracted from the total ρ_{xy} as described in equation 6.5. To do so we began by performing the linear fitting in a higher field region (> 1T). After linear fit, the slope and the intercepts provide the values of R_o and $R_s M_s$ respectively. The magnitude of AHE was 10 micro-ohm-cm at 2K shown in the inset of figure 6.6. The anomalous Hall conductivity (σ_{xy}^{AHC}) of the system is calculated by using the following equation:

$$\sigma_{xy}^{AHC} = \frac{\rho_{xy}}{(\rho_{xy}^2 + \rho_{xx}^2)} \tag{6.6}$$

Figure 6.7 shows the σ_{xy}^{AHC} vs.H in the temperature range of 2 K to 300 K. The value of AHC at 2 K is 83.5 S/cm is observed. A similar value of AHC is found for other systems

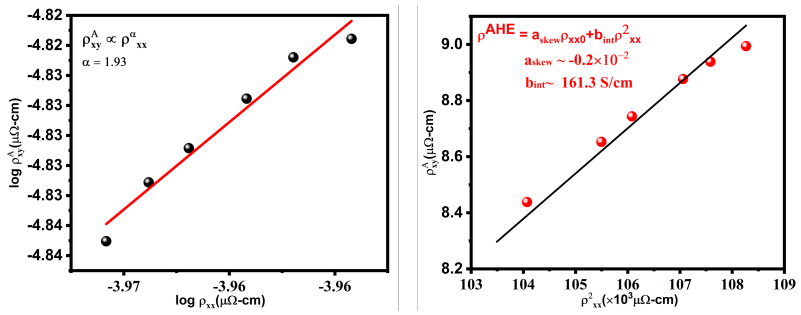

Fig. 6.7 (a) Scaling relation used in double logarithmic plot between ρ_{xy}^{A} and ρ_{xx} (black balls) and linear fitting is shown by red line.)

also. Particularly here the experimentally observed value of AHC is comparable with the reported by Xia et.al. viz; 87 S/cm. However, Gupta et. al. reported a considerably smaller value i.e. 53 S/cm at 5 K. The lower value observed by Gupta et. al. was due to the fact that compared to half-metallic ferromagnets (HMFs) and ferromagnetic metal, spin gapless semiconductor (SGSs) magnetic Heusler compounds are documented to exhibit a lower anomalous Hall conductivity (AHC). Understanding of the mechanism involved in AHE in the system is crucial for applying them in spintronics. Hence, to gain insight into the AHE and its underlying mechanism, both intrinsic and extrinsic, we have used a scaling model.

$$\rho_{xy} \propto \rho_{xx}^{\alpha} \tag{6.7}$$

These scaling models helps in determining the separate contributions coming from extrinsic and intrinsic mechanism as well as determining the dominating mechanism in AHE. In equation 6.7 if α = 1 then the extrinsic mechanism is solely responsible for the observation of AHE. If α =2 then it suggested that both intrinsic as well as side jump are responsible for the presence of AHE in the system. The combined contribution of intrinsic mechanism and side jump cannot be further extinguished. For the present system, the value of α = 1.93 after plotting the equation 6.7 on a logarithmic scale. This suggested that the intrinsic mechanism is dominating. The following scaling relation is used to determine

the separate contributions from extrinsic and intrinsic mechanisms.

$$\rho_{xy}^{AHE} = a\rho_{xx0} + b\rho_{xx}^{2} \tag{6.8}$$

Here, a shows the part that comes from extrinsic skew scattering, and b shows the parts that come from intrinsic and side jump scattering. After fitting the relation given above (6.8 the value of a and b is -0.003, 161.5 S/cm respectively as shown in figure 6.7. The experimentally observed AHC (viz 83.5 S/cm) is half of the value of theoretically obtained value after fitting (viz 161.5 S/cm). The disparity occurs because the intrinsic mechanism has an opposite nature to the extrinsic mechanism, as shown by the negative sign of a. It has been seen that other systems with half-metallicity have the same AHC Nag et al. (2022).

6.4 Conclusion

Here, we have reported the effect of antisite disorder on the magnetic and transport properties of the quarternary Heusler alloy *CoFeMnSn*. The XRD data analysis shows that the system is synthesized in type I configuration with partial disorder between the atoms of the system. The magnetization study confirmed that the system is room-temperature ferromagnetic, which makes it suitable for application purposes. The value of saturation magnetization is a non-integer value which is 4.3 μB/f.u. The non-integer value indicates the deviation of the system from Half metallicity. This deviation is due to antisite disorder present in the system. Further, the resistivity of the system decreases as the temperature increases, suggesting the semi-metallic behaviour. The transverse resistivity shows a similar nature to the magnetization of the system, suggesting the presence of anomalous Hall effect in the system. The value of anomalous hall conductivity is 83.5 S/cm which is larger due to the antisite disorder between the atoms. The anomalous Hall conductivity

confirms that the unusual Hall conductivity comes from the intrinsic contributions. The high transition temperature (T_C) and the consistent anomalous Hall conductivity up to room temperature make the material more practical for various applications.